Mesoporous Materials

Three-Dimensional Structure of Large-Pore Mesoporous Cubic *Ia*$\bar{3}$*d* Silica with Complementary Pores and Its Carbon Replica by Electron Crystallography**

*Yasuhiro Sakamoto, Tae-Wan Kim, Ryong Ryoo, and Osamu Terasaki**

Large-pore three-dimensional (3D) mesoporous silicas are among the most interesting mesoporous materials discovered in recent years, and they have attracted much attention for potential applications requiring easily accessible, uniform, large pores. Examples of these are SBA-15 (*p6mm*) and SBA-16 (*Im*$\bar{3}$*m*), which have cylindrical- and cage-type structures, respectively. It has been reported that hexagonally ordered large-pore mesoporous SBA-15 silica made by using a block copolymer contains complementary pores, while such pores were not found in MCM-41 with the same 2D hexagonal *p6mm* symmetry.[1] These complementary pores are arranged in a disordered way between the hexagonally ordered large-pore channels.

Recently, large-pore mesoporous silicas with a cubic *Ia*$\bar{3}$*d* structure were synthesized by using triblock copolymers as structure-directing agent under various synthesis conditions.[2] The mesoporous silica with a bicontinuous cubic structure of *Ia*$\bar{3}$*d* symmetry is composed of an enantiomeric pair of 3D mesoporous networks that are interwoven, as observed in the MCM-48 structure.

The structures of these highly ordered mesoporous materials can hardly be determined from powder XRD patterns alone, because the few reflections that are observed at low scattering angles are especially broad and overlap. Electron microscopy is the main tool for characterization of such structures. The advantage over XRD is the stronger interaction of electrons with matter, which enables us to obtain structural information from a single crystal with only a few hundred unit cells. In electron crystallography (EC) the phases and amplitudes of the structure factors are obtained by Fourier transformation of high-resolution TEM (HRTEM) images. By calculating the inverse Fourier transform of the structure factors, a 3D electrostatic potential distribution of the structure can be obtained. This is another advantage compared to traditional single-crystal XRD. Based on the 3D electrostatic potential distribution of the structure, direct information on the detailed structures inside the mesoporous crystals such as diameter, shape, and connectivity of the pores can be obtained.[3]

Herein we report on the structure of the large-pore mesoporous silica with cubic *Ia*$\bar{3}$*d* symmetry after removal of the surfactant by calcination and, in particular, on its ordered complementary pores between two independent channel systems, determined by using EC methods. Furthermore, the structure of its carbon replica, made by using this large-pore mesoporous silica as a hard template and then removing the template, is reported.

Figure 1 shows HRTEM images of mesoporous silica with *Ia*$\bar{3}$*d* symmetry taken with the incident beam parallel to the [100] (a), [110] (b), and [111] (c) directions. Corresponding Fourier diffractograms (FDs) are inset in each image. The FDs of these images clearly show the reflection conditions: hkl, $h+k+l=2n$; $0kl$, k and $l=2n$; hhl, $2h+l=4n$ and $l=2n$; $00l$, $l=4n$. From these observations, the space group symmetry was uniquely determined to be *Ia*$\bar{3}$*d*. The lattice constant derived from the 211 spot of the electron diffraction (ED) pattern with [111] incidence is 2.3×10^2 Å. Figure 2a shows the XRD pattern of the specimen; the lattice constant obtained from the 211 peak position is 2.38×10^2 Å.

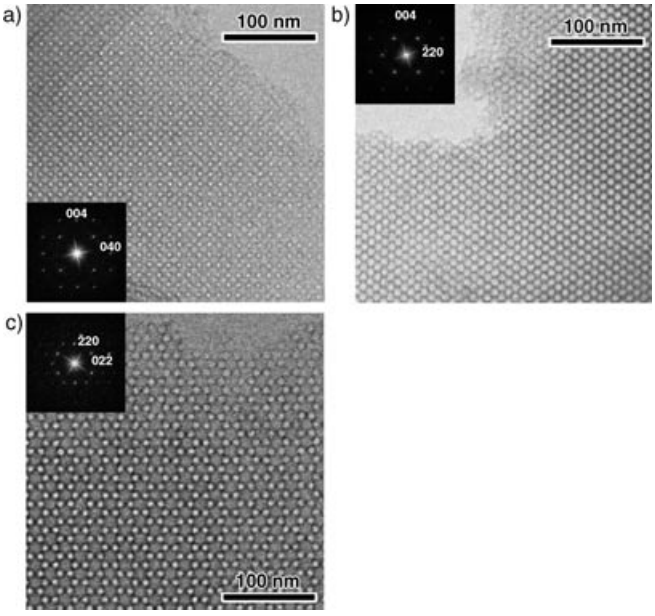

Figure 1. HRTEM images of the large-pore mesoporous silica taken with the incident beam parallel to the [100] (a), [110] (b), and [111] (c) directions; corresponding Fourier diffractograms are inset in each image.

These images taken with three different axes, [100], [110], and [111] were used for the reconstruction process. The resolution of the reconstructed distribution was limited to 26.2 Å, although some images showed a few higher resolution

[*] Dr. Y. Sakamoto, Prof. Dr. O. Terasaki
Structural Chemistry
Arrhenius Laboratory
Stockholm University
10691 Stockholm (Sweden)
Fax: (+46) 8-162-379
E-mail: terasaki@struc.su.se
T.-W. Kim, Prof. Dr. R. Ryoo
National Creative Research Initiative Center for
Functional Nanomaterials and
Department of Chemistry (School of Molecular Science-BK21)
Korea Advanced Institute of Science and Technology
Daejeon, 305-701 (Korea)

[**] This work was supported by the Swedish Natural Science Council (VR) and the Japan Science and Technology Agency (JST).

Supporting information for this article is available on the WWW under http://www.angewandte.org or from the author.

 DOI: 10.1002/anie.200460449

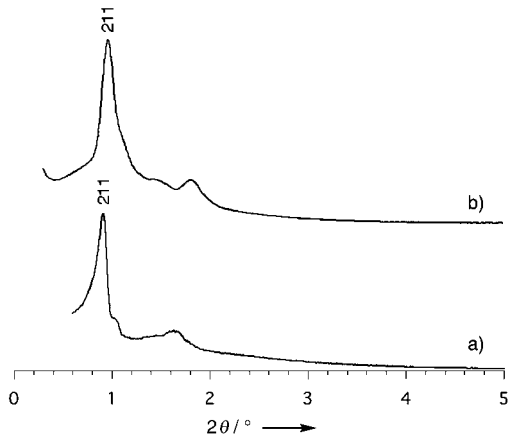

Figure 2. XRD of the large-pore mesoporous silica (a) and the carbon replica (b).

spots. Those for 25 reflections were determined in 33 unique reflections within the resolution limit, that is, $h^2+k^2+l^2=78$. A summary of observed 3D crystal structure factors after normalization by common reflections and correction of the contrast transfer function (CTF) is given in Table 1. The 512, 631, 543, 721, 732, 741, 653, and 813 reflections cannot be obtained from [100], [110], and [111] incidences. However, it was confirmed in ED studies by tilting the crystal that the intensities of all of these reflections were very weak. The values of other vacant cells in Table 1 were ignored (i.e., $S/N<3$). From the structure factors, the 3D electrostatic potential map (arbitrary scale) was uniquely obtained by calculating the inverse Fourier transform of the structure factors. Figure 3 shows the 3D electrostatic potential maps of the mesoporous silica. The bright parts correspond to the pore, and dark parts to the silica wall. The sections are parallel to the (010) plane at $y=0$ (a) and 0.125 (b) and the (111) plane through the origin, $x=y=z=0$ (c).

A threshold value that defines the boundary between the silica wall and the pore must be determined in order to obtain the 3D pore structure of the mesoporous silica from 3D electrostatic potential maps. This value corresponds to the potential density constant, where 1 represents the pore and 0 the silica wall. The total pore volume of mesoporous silica as determined from N_2 adsorption/desorption measurements is 1.149 $cm^3 g^{-1}$, calculated from the amount adsorbed at a relative pressure of 0.99. Assuming a density of the silica wall of 2.20 $g cm^{-3}$, the pore volume fraction corresponds to 71.7 % and a threshold value of 0.218 (see Supporting Information 1). Figure 4a shows the 3D pore structure of the mesoporous

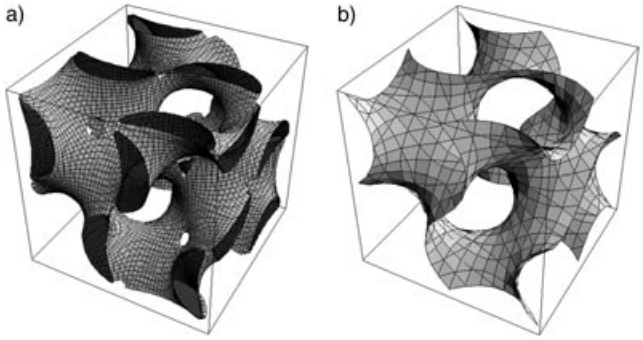

Figure 4. Schematic drawing of 3D arrangement of pores for a pore fraction of 71.7% and a threshold value of 0.218 (a) and G-surface (b).

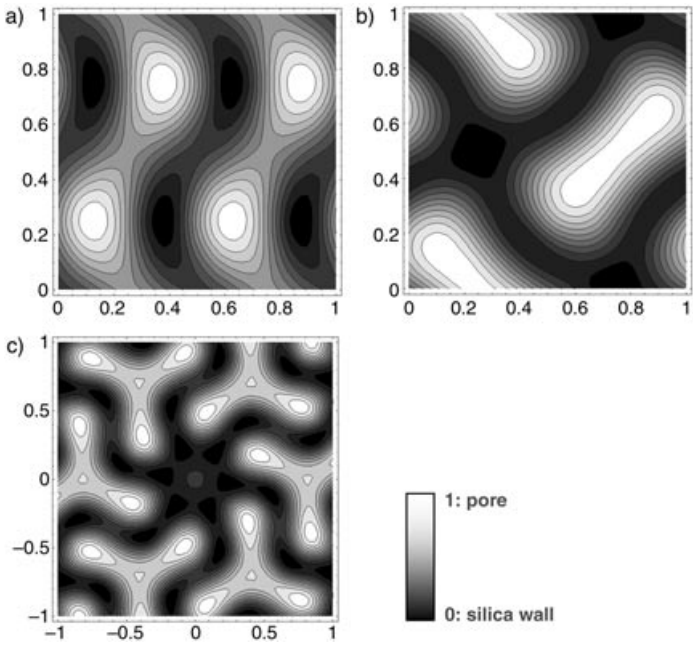

Figure 3. Electrostatic potential maps of the large-pore mesoporous silica. Sections parallel to the (010) plane at $y=0$ (a) and 0.125 (b), and the (111) plane through the origin (c). Bright parts correspond to the pores, and dark parts to the silica wall. One unit cell is shown for each orientation, where $a=2.3\times10^2$ Å.

silica with this threshold value. It is clear that the silica wall exactly follows the G-surface (Figure 4b). The pore diameter and wall thickness of the silica estimated from the 3D pore structure are 83 and 35 Å, respectively. Complementary pores of 17 Å were found to form interconnections between the two main channel systems at a special flat point of the G-surface, that is, $\bar{3}$ position on the 3-fold axis, 16*a* site (Wyckoff notation) of the space group $Ia\bar{3}d$ (see Supporting Information 2). In contrast to SBA-15, these complementary pores are ordered.

Figure 5 shows N_2 adsorption/desorption isotherm data. The isotherm is of type IV, which is typical for mesoporous materials, and it is similar to those observed for cylindrical-type mesoporous structures.[2] The isotherm is characterized by a sharp capillary condensation step in the adsorption branch at high relative pressures ($p/p_0=0.75$–0.8), and an H1 hysteresis loop in the desorption branch of the isotherm. The pore diameter calculated by the BJH method is 78 Å. On the other hand, the DFT model assuming a cylindrical pore geometry[4] gives diameters of 18 Å for the complementary pores and 124 Å for the main pores. The t-plot analysis reveals the presence of complementary pores with a micropore surface area of 69.0 $m^2 g^{-1}$ (see Supporting Information 3). The BJH model is known to underestimate pore size,[4] and this explains the difference in main pore diameter between the BJH and DFT methods of pore size analysis. The

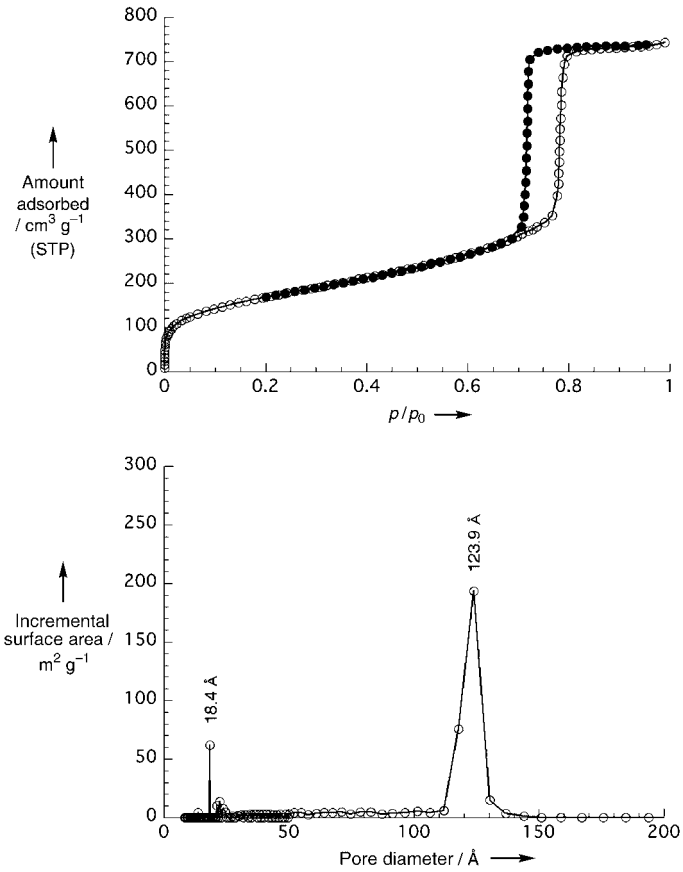

Figure 5. N_2 adsorption(●)/desorption(○) isotherm (a) and pore size distribution (b).

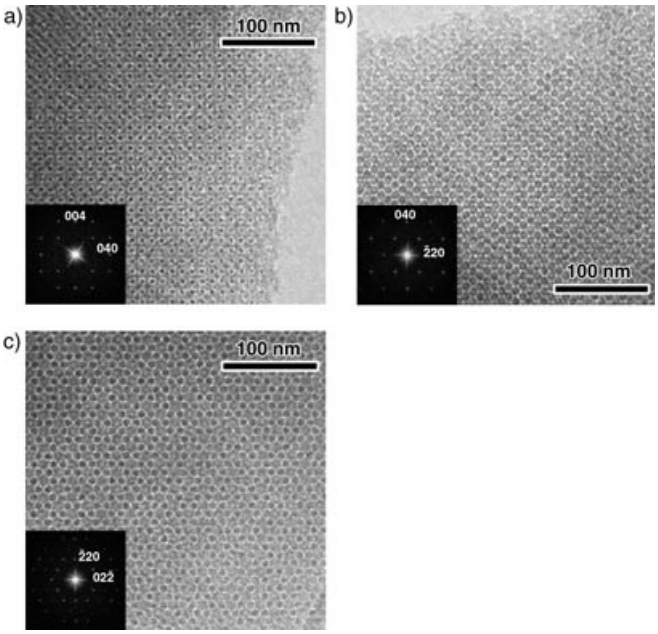

Figure 6. HRTEM images of the carbon replica taken with the incident beam parallel to the [100] (a), [110] (b), and [111] directions; corresponding Fourier diffractograms are inset in each image.

complementary-pore size derived from the DFT model is in good agreement with that from the 3D reconstructed structure. The BET surface area S_{BET} is about 600 $m^2 g^{-1}$.

Figure 6 shows HRTEM images along the [100], [110], and [111] directions of the carbon replica made by using the mesoporous silica as template. Corresponding FDs are inset in each image. The FDs clearly show the extinction rule. From these observations, the space-group symmetry was uniquely determined to be $Ia\bar{3}d$, which is the same as that of the mesoporous silica template. These images show well-ordered carbon structures and inverse contrasts with respect to those of the mesoporous silica. The lattice constant obtained from the 211 spot of the ED pattern with [111] incidence is 2.2×10^2 Å. Figure 2b shows the XRD pattern of the carbon replica, and the lattice constant obtained from the 211 peak position is 2.26×10^2 Å. The 3D structure of the carbon replica was determined from these three images by EC in the same way as the 3D reconstruction of the mesoporous silica. The 3D structure factors were collected in the range of 23.5 Å, and those for 27 reflections were determined as shown in Table 1. Note that the phases of the first ten structure factors are exactly opposite to those of the mesoporous silica. The pores of the hard template, both right- and left-handed channel systems, are filled uniformly by carbon, and therefore Babinet's principle applies. Deviation from Babinet's principle for reflections with larger scattering vectors may be attributed to the minor changes together with lattice contraction after dissolution of silica.

The electrostatic potential map of the carbon replica was uniquely obtained by calculating the inverse Fourier transform of the structure factors. To obtain the structure of the carbon, the threshold value of the boundary between carbon and space was chosen by taking account of carbon without overlapping the silica wall of the large-pore mesoporous silica, which is defined by a threshold value of 0.218. In this case, the carbon has the threshold value of 0.648 (see Supporting Information 1), whereby the boundary between the silica wall and the pores of the large-pore mesoporous silica is same as that between carbon and the space of the carbon replica. Hence, the carbon replica is continuously formed in the space of the mesoporous silica (see Supporting Information 4).

The 3D structure of large-pore mesoporous silica was obtained by the Fourier transform of the structure factors, which were extracted from the HRTEM images. Complementary pores through the silica wall at the special flat point of the G-surface between two channel systems on the threefold axis (16*a* site) was found. The size of the complementary pore is sensitive to the threshold value, which defines the boundary between the silica wall and the spaces, and also dependent on silica density. The diameter is 17 Å for an assumed silica wall density of 2.20 $g cm^{-3}$. With decreasing silica density, the size of complementary pore becomes smaller, and at a silica wall density of 2.05 $g cm^{-3}$, which corresponds to a pore volume fraction of 70.2% and a threshold value of 0.227, the complementary pore is closed.

The 3D structure of the carbon replica was also reconstructed. The carbon replica follows the pore space of the mesoporous silica continuously and retains the $Ia\bar{3}d$ symme-

Table 1: Crystal structure factors obtained by electron crystallography.

		Large-pore mesoporous silica[a]			Carbon replica[b]		
hkl	$h^2+k^2+l^2$	*d* [Å]	$\lvert F_{hkl}\rvert / \lvert F_{211}\rvert$	phase	*d* [Å]	$\lvert F_{hkl}\rvert / \lvert F_{211}\rvert$	phase
211	6	94.4	100.00	π	90.0	100.00	0
220	8	81.7	34.69	π	78.0	47.92	0
321	14	61.8	6.33	0	58.9	11.04	π
400	16	57.8	6.61	0	55.1	27.52	π
420	20	51.7	4.63	0	49.3	13.58	π
332	22	49.3	3.89	π	47.0	18.97	0
422	24	47.2	1.48	π	45.0	9.73	0
431	26	45.3	0.70	π	43.2	6.52	0
521	30	42.2			40.3		
440	32	40.9	0.46	0	39.0	0.95	π
532	38	37.5	0.19	0	35.8	0.57	π
611	38	37.5	0.51	π	35.8	1.82	π
620	40	36.6	0.31	π	34.9	1.04	π
541	42	35.7	0.34	0	34.0	0.20	π
631	46	34.1			32.5		
444	48	33.4	0.32	0	31.8	1.85	0
543	50	32.7			31.2		
640	52	32.1	0.27	π	30.6	0.69	π
552	54	31.5	0.16	0	30.0	0.30	0
633	54	31.5	0.20	0	30.0	0.52	0
721	54	31.5			30.0		
642	56	30.9	0.20	0	29.5	0.69	0
651	62	29.4	0.02	π	28.0	0.26	0
732	62	29.4			28.0		
800	64	28.9	0.13	0	27.6	0.24	0
741	66	28.5			27.1		
820	68	28.0	0.14	0	26.7	0.13	0
653	70	27.6			26.4		
660	72	27.2	0.11	π	26.0	0.17	π
822	72	27.2	0.04	π	26.0	0.17	π
743	74	26.9	0.06	π	25.6		
831	74	26.9			25.6		
752	78	26.2	0.14	π	25.0	0.11	0
840	80	25.8			24.7		
842	84	25.2			24.1		
655	86	24.9			23.8	0.15	0
761	86	24.9			23.8	0.21	0
921	86	24.9			23.8		
664	88	25.6			23.5	0.16	0

[a] $a = 2.3 \times 10^2$ Å. [b] $a = 2.2 \times 10^2$ Å.

try of the template. This is responsible for the complete replication by carbon with the same symmetry, which is a notable difference from the previously synthesized CMK-1 carbon.[5]

Experimental Section

The large-pore mesoporous silica with cubic $Ia\bar{3}d$ symmetry was prepared by following the procedure using the triblock ethylene oxide (EO)–propylene oxide (PO)–EO copolymer Pluronic P123 ($EO_{20}PO_{70}EO_{20}$, $M_{av} = 5800$), butanol, and tetraethyl orthosilcate (TEOS).[2f] Replication of the silica was performed by following a known synthesis procedure, with the modification of using furfuryl alcohol instead of sucrose as the carbon source.[6]

Powder XRD patterns were recorded with $Cu_{K\alpha}$ radiation ($\lambda = 1.5406$ Å) at 50 kV and 30 mA (1.5 kW) in step-scan mode (fixed time) with a small divergent slit.

Transmission electron microscopy (TEM) was conducted with a JEOL-3010 microscope operating at 300 kV ($C_s = 0.6$ mm, resolution 1.7 Å). Images were recorded with a CCD camera (model Keen View, SIS analysis, size 1024×1024 pixels, pixel size 23.5×23.5 μm) at 30000–50000× magnification under low-dose conditions.

The N_2 adsorption/desorption measurements were performed at 77 K on an ASAP2020 Micromeritics Instrument. The sample was degassed for 6 h at 423 K and 0.3 kPa. The BET specific surface area S_{BET} was calculated from adsorption branches in the relative pressure range from 0.05 to 0.3. The total pore volume was estimated from the amount adsorbed at a relative pressure of 0.99. Pore size distribution curves were derived by DFT, as developed recently by Ravikovitch et al.,[4] by assuming a cylindrical pore geometry.

Received: April 26, 2004

Keywords: carbon · electron crystallography · mesoporous materials · silica

[1] a) R. Ryoo, C. H. Ko, M. Kruk, V. Antochshuk, M. Jaroniec, *J. Phys. Chem. B* **2000**, *104*, 11465; b) Z. Liu, O. Terasaki, T. Ohsuna, K. Hiraga, H. J. Shin, R. Ryoo, *ChemPhysChem* **2001**, *2*, 229; c) S. H. Joo, S. J. Choi, I. Oh, J. Kwak, Z. Liu, O. Terasaki, R. Ryoo, *Nature* **2001**, *412*, 169; d) O. Terasaki, Z. Liu, T. Ohsuna, H. J. Shin, R. Ryoo, *Microsc. Microanal.* **2002**, *8*, 35.

[2] a) X. Liu, B. Tian, C. Yu, F. Gao, S. Xie, B. Tu, R, Che, L. Peng, D. Zhao, *Angew. Chem.* **2002**, *114*, 4032; *Angew. Chem. Int. Ed.* **2002**, *41*, 3876; b) Y. T. Chan, H. P. Lin, C. Y. Mou, S. T. Liu, *Chem. Commun.* **2002**, 2878; c) H. Yang, Q. Shi, X. Liu, S. Xie, D. Jiang, F. Zhang, C. Yu, B. Tu, D. Zhao, *Chem. Commun.* **2002**, 2842; d) K. Flodström, V. Alfredsson, N. Källrot, *J. Am. Chem. Soc.* **2003**, *125*, 4402; e) S. Che, A. E. Garcia-Bennett, X. Liu, R. P. Hodgkins, P. A. Wright, D. Zhao, O. Terasaki, T. Tatsumi, *Angew. Chem.* **2003**, *115*, 4060; *Angew. Chem. Int. Ed.* **2003**, *42*, 3930; f) F. Kleitz, S. H. Choi, R. Ryoo, *Chem. Commun.* **2003**, 2136.

[3] a) A. Carlsson, M. Kaneda, Y. Sakamoto, O. Terasaki, R. Ryoo, S. H. Joo, *J. Electron Microsc.* **1999**, *48*, 795; b) Y. Sakamoto, M. Kaneda, O. Terasaki, D. Zhao, J. M. Kim, G. D. Stucky, H. J. Shin, R. Ryoo, *Nature* **2000**, *408*, 449; c) M. Kaneda, T. Tsubakiyama, A. Carlsson, Y. Sakamoto, T. Ohsuna, O. Terasaki, S. H. Joo, R. Ryoo, *J. Phys. Chem. B* **2002**, *106*, 1256; d) Y. Sakamoto, I. Diaz, O. Terasaki, D. Zhao, J. P. Pariente, J. M. Kim, G. D. Stucky, *J. Phys. Chem. B* **2002**, *106*, 3118.

[4] a) P. I. Ravikovitch, G. L. Haller, A. V. Neimark, *Adv. Colloid Interface Sci.* **1998**, *76–77*, 203; b) P. I. Ravikovitch, A. V. Neimark, *Langmuir* **2000**, *16*, 2419.

[5] R. Ryoo, S. H. Joo, S. Jun, *J. Phys. Chem. B* **1999**, *103*, 7743.

[6] S. Jun, S. H. Joo, R. Ryoo, M. Kruk, M. Jaroniec, Z. Liu, T. Ohsuna, O. Terasaki, *J. Am. Chem. Soc.* **2000**, *122*, 10712.

